**Final Project Report**

**Dec. 12, 2001**

**Grant No.**: DE-FG07-99ER15019

**Project No**.: 70121
**Principal Investigator**: Carrick M. Eggleston, Department of Geology and Geophysics, University of Wyoming.
**Project Period**: 9/15/99 to 9/14/02; no-cost extended to 9/14/03
**Budget Period covered by this Report**: Entire project period
**Project Title**: "The Influence of Calcium Carbonate Grain Coatings on Contaminant Reactivity in Vadose Zone Sediments".

Our collaborators on the overall project are Stanford University and Pacific Northwest National Laboratory; overall project leader is Dr. John Zachara, PNNL.

**Executive Summary:**

The purpose of this study was to better understand the chemical interactions between dissolved aqueous contaminants and carbonate minerals occurring as coatings on mineral grains in the vadose zone beneath the Hanford reserve. This information is important for construction of improved reactive transport models intended to predict the subsurface migration of contaminants.

We made improvements to the hydrothermal atomic force microscope (HAFM) design to be used in this project. The original HAFM was built with funding from the U.S. DOE, Office of Basic Energy Sciences. Improvements include operating limits of 70 bars and 170°C, from an original limit of 12 bars and 150°C. This product is patented. We completed a series of studies of magnesite, $MgCO_3$, because this mineral is structurally equivalent to calcite but reacts much more slowly, allowing us to study carbonate reactivity under pH conditions (i.e., low pH) that are much more problematic for studies of calcite but which are nevertheless relevant to in-situ conditions. We found that dissolving magnesite exhibits a dramatic change in step orientation, and therefore etch pit shape, as pH is lowered through 4.2 to 3 and 2. This change in step orientation is NOT accompanied by an increase in step velocity with decreasing pH. We also found that, after growing magnesite on a magnesite substrate, the newly grown magnesite dissolved much more readily than the underlying substrate magnesite, and exhibited far larger etch pit densities. This effect may have been related to the presence of an Fe impurity in the growth solutions.

We studied the dissolution of magnesite and calcite (104) surfaces under a wider variety of conditions with a new hydrodynamically defined hydrothermal AFM fluid cell, and we have observed the precipitation of a strontium-containing carbonate phase on dissolving calcite. We have applied the advection-diffusion equation coupled to proposed homogeneous and heterogeneous kinetic models to test rate laws for dissolution observed by HAFM.

Our main conclusions in the magnesite studies are that step density, rather than step velocity, is a strong function of pH near the surface and that the step orientation is sensitive to pH. In these studies, we definitively demonstrate that diffusive mass transport is only important at very low fluid velocities for magnesite, but that studies of calcite dissolution are generally in the mixed transport-kinetics controlled regime (even at high fluid velocities) where quantitative information can only be obtained by accounting for the transport components. We also have found that alkaline earth carbonate secondary precipitate formation on calcite surfaces significantly alters the net flux of $Ca^{2+}$ and may passivate the $CaCO_3$ surface from further reaction.

The research has so far resulted in 6 conference presentations and 3 published journal articles, with several manuscripts still in preparation. The project supported graduate student Briana Deeds and postdoctoral researcher Steven R. Higgins.

**Comparison of accomplishments with the goals and objectives of the project:**

All major goals of the originally proposed project have been met in terms of accomplished research with the exception of studies on the interaction of chromate with calcite, which are ongoing. Manuscripts relating to step velocity and orientation have been published. Manuscripts relating to Sr and Co interaction with calcite are in preparation. Interruption of progress because of

graduate student Briana Deeds' personal circumstances occurred, work resumed at full efficiency. This led to a no-cost extension, but progress is ongoing and productive at the present time, and submission of further manuscripts is anticipated within the year.

**Publications:**


Jordan, G., Higgins, S.R., Eggleston, C.M., Knauss, K.G. and Schmal, W.W. (2001) Dissolution kinetics of magnesite in acidic aqueous solution, a hydrothermal atomic force microscopy (HAFM) study: Step orientation and kink dynamics. Geochimica et Cosmochimica Acta 65(23), 4257-4266.

Higgins S. R., Jordan G., and Eggleston C. M. (2002) Dissolution kinetics of magnesite in acidic aqueous solution, a hydrothermal atomic force microscopy (HAFM) study: Step kinetics and dissolution flux. *Geochimica et Cosmochimica Acta* 66(18), 3201-3210.

Higgins S. R., Boram L. H., Eggleston C. M., Coles B. A., Compton R. G. and Knauss K. G. (2002) Dissolution kinetics, step and surface morphology of magnesite (104) surfaces in acidic aqueous solution at 60°C by atomic force microscopy under defined hydrodynamic conditions, *Journal of Physical Chemistry B* 106, 6696-6705.


**Conference presentations:**


Greer B., Higgins S. R., Eggleston C. M., Boram L. H., Knauss K. G. (2002) Study of heterogeneous kinetics at calcite surfaces in the presence of strontium using atomic force microscopy, contributed talk at the ACS National Meeting, April 2002, Orlando, FL.

Higgins, S. R., Greer, B., Boram, L. H., Eggleston, C. M., Jordan, G., Knauss, K. G. (2001) Study of heterogeneous kinetics at carbonate mineral surfaces using hydrothermal atomic force microscopy. ACS National Meeting, August 2001, Chicago, IL.

Higgins, S. R., Greer B., Boram L. H., Eggleston C. M., and Knauss K. G. (2001) Hydrothermal Scanning Probe Microscopy and its Application to Problems in Heterogeneous Kinetics: Adventures (and Misadventures) at Mineral Surfaces. Invited speaker at the 11th Annual V. M. Goldschmidt Conference, Hot Springs, VA, May 2001.

Higgins, S. R., Boram, L. H., Greer, B., Coles, B. A., Compton, R. G., Eggleston, C. M., Knauss, K. G. (2001) Hydrodynamic atomic force microscopy and its applications to carbonate mineral dissolution. Materials Research Society Meeting, San Francisco, CA, April, 2001.

Eggleston, C.M. and Higgins, S.R. (2001) In-Situ Observation of Crystal Growth Processes by Atomic Force Microscopy: New Methods in Hydrothermal Surface Science. Invited presentation at the Geophysical Laboratory, Carnegie Institute of Washington, Feb. 2001.

Higgins, S., Jordan, G., Coles, B., Compton, R., Eggleston, C., Knauss, K., Boro, C. (2000) Studies of the dissolution of magnesite(104) in acidic aqueous solutions: A new approach using hydrothermal scanning probe microscopy under controlled hydrodynamic conditions. Contributed talk at the 10th Annual V. M. Goldschmidt Conference, Oxford, UK. Journal of Conference Abstracts, 5(2), 513.

**Description and discussion of research results:**

The vadose zone at Hanford is of particular geochemical interest because $CaCO_3$ coated sediments increase the importance of carbonate reactions. Coatings may retard $^{90}Sr$ and $^{60}Co$ migration through incorporation into existing or precipitating carbonates. Carbonate coatings may cover iron hydroxide, known to complex $CrO_4^{2-}$ (Drever, 1997) potentially facilitating the migration of chromate. Chromate may complex calcium, and be incorporated into precipitating carbonates, retarding its migration. Each contaminant poses an environmental hazard; $^{90}Sr$, and $^{60}Co$ are radioactive with respective half-lives of 29.1 years, and 5.27 years (Lide,1995), while $CrO_4^{2-}$ is a biocide and carcinogen (Nriagu,1988). Large volumes of waste have leached through the vadose zone causing ground water contamination, as revealed by elevated Tc in ground water. Sr, Co, and $CrO_4^{2-}$ are all contaminants of concern in the vadose zone (US DOE, 2000). $Sr^{2+}$ and $Co^{2+}$ may undergo incorporation into existing carbonates, or formation of a contaminant rich carbonate precipitate, in the presence of a carbonate source (Lorens, 1981, Reeder 1983; Pingitore, et al.,1992) in Hanford's vadose zone.

While both carbonate growth and dissolution influence Sr, Co, and Cr transport in this vadose zone, this study focuses on settings of dissolving calcite coupled with growth of contaminant carbonate (strontianite or cobalticalcite) such that the calcite serves to remove Sr and Co from solution. In the case of chromate, we focus on incorporation of chromate into the carbonate structure (this is unlikely to be a precipitation process). Specifically, $CaCO_3$ coupled mass transport/kinetics during dissolution in the presence of Sr, Co, and $CrO_4^{2-}$ is addressed with hydrodynamically controlled AFM (HAFM) experiments. Because waste solutions are typically at relatively high temperature, these experiments were performed at 40º C. The effect of Strontium, Cobalt, and Chromate at various concentrations on calcite $\{10\bar{1}4\}$ dissolution kinetics under controlled hydrodynamic conditions, as a function of known fluid velocity, allows us to identify an appropriate rate law for each experimental condition, and create a near surface reactant concentration map through backwards implicit finite difference (BIFD) modeling. Calcite dissolution subsequently increases near surface saturation with respect to calcite, cobalticalcite, aragonite, strontianite, and calcium chromate species. Existence and distribution of precipitates was confirmed by SEM or Electron Microprobe. Solid solution of potential precipitates is addressed following ideas presented in Casey et al., 1996, Pina, et al. (2000), and Astilleros et al., 2002) using the concentrations provided from BIFD modeling. Consideration of

dissolution flux from calcite as a function of step velocity will facilitate the comparison of this experiment with similar AFM experiments.

*Sample and Solution Preparation*

0.05 millimolar to 5 mM strontium, cobalt, and chromate are made in a 0.1 molar sodium nitrate solution. Strontium, cobalt, or chromate is added as a dissolved salt ($SrNO_3$, $CoNO_3$, and $Na_2Cr_2O_7*2H_2O$) from a stock solution. Rinsing the HAFM reservoir and plumbing with experimental solution before sealing helps ensure purity. Once sealed, the fluid containing reservoir is pressurized (10 p.s.i.), heated to 40°C and left overnight. Solution chemistry can be modeled using MinteqA2 assuming atmospheric $CO_2$ pressure provides the only source carbonate activity.

Before cleaving a calcite sample and sealing the fluid cell a cantilever is secured to the fluid cell top which acts as both fluid cell jet and cantilever holder. A gold clip and screw hold the cantilever in place. The position of the cantilever tip with respect to the jet inside edge corner nearest the cantilever substrate is photographed so tip distance from the jet can be determined. Knowing the distance from jet to tip allows one to identify the area of interest from a surface concentration map after modeling, where modeled flux should equal empirical flux upon selection of an appropriate rate law.

For each experiment a calcite crystal is cleaved with a razor and placed fresh side $\{10\bar{1}4\}$ up in the HAFM fluid cell, noting the orientation for reference. A 0.1 micron gold wire secures the crystal to the piezo stage. Before sealing the fluid cell with the anodized titanium fluid jet/cantilever unit, plumbing leading to the fluid cell is flushed filling tubing with reservoir solution. Once assembled, the fluid cell and pre-heater are brought to 40°C before the experiment begins.

*Data Collection*

Calcite dissolution flux from the $\{10\bar{1}4\}$ cleavage plane is empirically determined over a range of aqueous impurity concentrations and flow rates by counting steps passing a point in sequential HAFM images of known frequency. Step velocity can be determined by comparing change in step angles in up and down scans of the same images. It is crucial in these experiments to find a consistent step train; keeping track of competing and interacting steps in a

step counting situation can lead to skewed data. Using a consistent step train means steps being observed are all the same orientation, and likely emanating from a single large pit. Data in these experiments are obtained from obtuse [ $48\bar{1}$ ] unless otherwise noted. Sets of 5-20 sequential images of steps on the calcite are collected at several flow rates for the inlet $Sr^{2+}$ or $Co^{2+}$. Calcite crystals are analyzed for cobalt, and strontium by SEM and/or microprobe after the HAFM experiment to look for evidence of precipitation on the crystal surface.

**Results and Discussion:**

Step velocity is best determined by equations 1 and 2 (Land, et al., 1997) where □T, □D, and □U are the true angle of the step with respect to horizontal, the angle with respect to horizontal during down scan and the angle with respect to horizontal during up scan, R is scan rate in lines per second, N is the number of scan lines per HAFM image, and S is scan size. Figure 1 shows step velocity's dependence on flow rate at two Sr inlet concentrations, a clear indication of mass transport control.

$$\square\square = \cot^{-1}[(\cot \square D + \cot \square U)/2] \quad (1)$$

$$v = RS/2N[\cot \square D - \cot \square U]\sin \square T \quad (2)$$

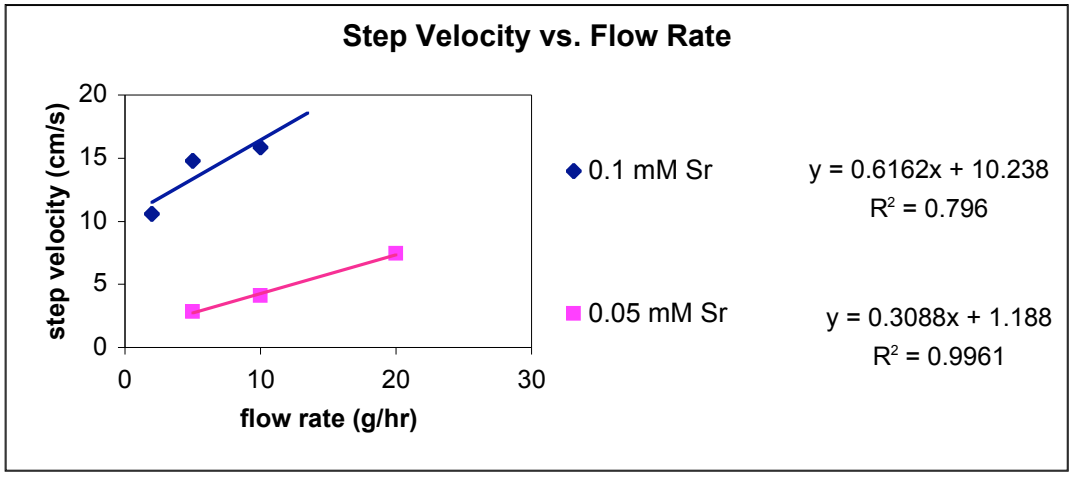


Figure 1. Step velocity, calculated by eqs. 1 and 2, as a function of flow rate for $Sr^{2+}$ concentrations of 0.05 and 0.1 mM.

These results, however, contrast with those from Lea et al, 2001, who observed that obtuse steps decrease in speed with increasing strontium concentration, while acute steps increase in speed with increasing strontium concentration.

Dissolution flux is calculated (eq. 3) by multiplying the number steps counted (n) with the height (*h*), 3 Å for calcite, then dividing by molar volume $V_m$, 36.9 $cm^3$/mol, and time past (s) in the sequential images gives flux ($mol*s^{-1}*cm^{-2}$). (Teng, et al., 2000; Gratz, et al., 1993)

$$J= n*h/(V_m*s) \qquad (3)$$

The experimental reaction rate can then be compared with a rate calculated through hydrodynamic modeling; to determine which rate law best fits the empirical flux (Higgins, et al., 2002). Empirically determined calcite dissolution fluxes at disparate flow rates for several inlet strontium concentrations are presented in figure 2. Calcite dissolution fluxes at several flow rates from an inlet cobalt concentration of 0.1mM are presented in figure 3. A clear trend is evident between mass transport and calcite dissolution flux in both strontium and cobalt containing solutions. Figure 2 also demonstrates a trend of increasing calcite dissolution flux with increasing inlet strontium concentrations.

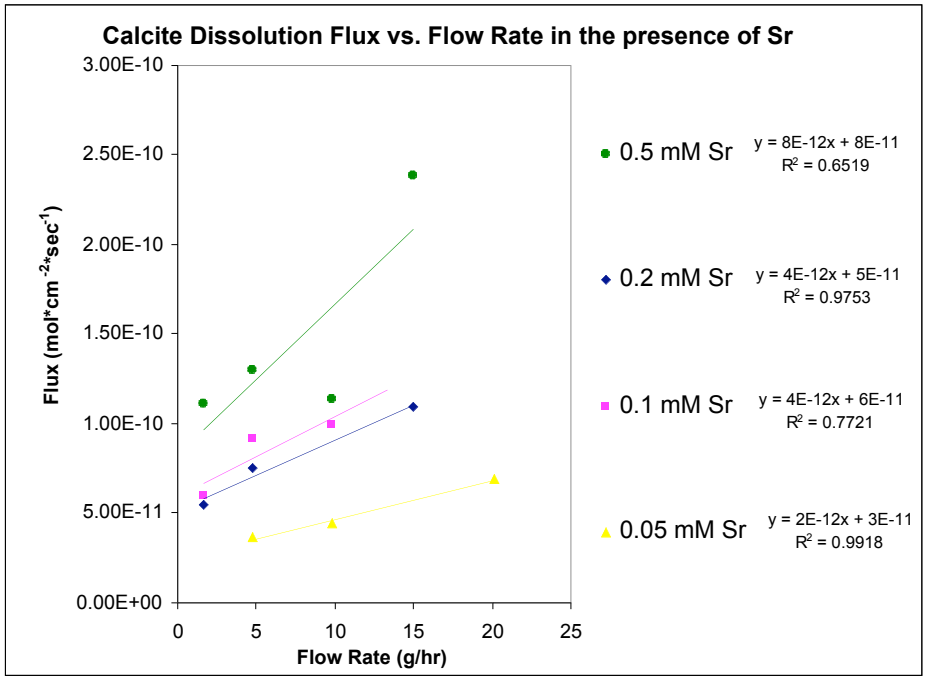


Figure 2. Calcite dissolution flux as a function of flow rate in the presence of inlet $Sr^{2+}$ concentrations ranging from 0.05 to 0.5 mM.

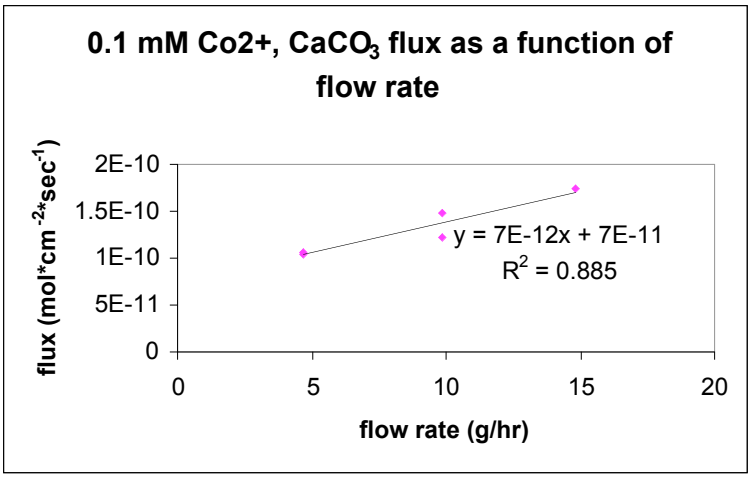


Figure 3. Calcite dissolution flux as a function of flow rate for $Co^{2+}$ inlet concentration equaling 0.1 mM . Data are from two different experiments with identical inlet

*Hydrodynamic Modeling of Calcite Flux*

The point of hydrodynamic modeling is the creation of reactant concentration maps near the calcite surface that can be used in further considering surface processes. A rate law must be chosen which defines flux from the calcite surface in order to model near surface concentrations of reactants. When the flux produced by the model in the scan area equals the experimentally determined flux we the chosen rate law sufficiently describes the mechanism at work

The general form of the advective-diffusion equation is presented in equation 4, where C is the concentration of a reactant, t is time, $D_C$ is the diffusion coefficient of reactant C, and $v_x$, $v_y$, and $v_z$ are fluid velocities in the x, y, and z directions. Directions x and z are parallel to the plane of the crystal parallel and perpendicular to the primary flow direction respectively, while direction y extends upward and perpendicular from the plane of the crystal.

$$\frac{\partial[C]}{\partial t} = D_C \nabla^2[C] - \left[ v_x \frac{\partial[C]}{\partial x} + v_y \frac{\partial[C]}{\partial y} + v_z \frac{\partial[C]}{\partial z} \right] \qquad (4)$$

If fluid velocities are known, equation 4 may be solved numerically using the backwards implicit finite difference model (BIFD) with key approximations:

$$\partial^2 C/\partial y^2 = (C_{j+1,k+1} - 2C_{j,k+1} + C_{j-1,k+1}/(\Delta y)^2$$

$$\partial C/\partial y = C_{j,k+1} - C_{j-1,k+1}/\Delta y$$

where j corresponds to increments the y direction, J refers to the last of the y increments.

Fluid velocities for the fluid jet's laminar flow have already been modeled by Compton et al, 1990, and are available on the internet. Once x and y fluid velocity vectors are combined via a bicubic spline routine into one fluid velocity vector d, and assuming that the net change in concentration with time for each spatial increment is zero, the advective diffusion equation simplifies to eq. 5.

$$0 = D(C_{j+1,k+1} - 2C_{j,k+1} + C_{j-1,k+1}/(\Delta y)^2) - v_y\,(C_{j,k+1} - C_{j-1,k+1}/\Delta y) - v_d\,(C_{j,k+1} - C_{j,k}/\Delta d) \qquad (5)$$

Further simplification leads equation 6,

$$C_{j,k} = aC_{j-1,k+1} + bC_{j,k+1} + cC_{j+1,k+1} \qquad (6)$$

where: $_y = D/(\Delta y)^2$, $_v_y = v_y/\Delta y$, $_v_d = v_d/\Delta d$

$$a = -(_y + _v_y)/_v_d,$$

$$b = (2_ + _v_y + _v_d)/_v_y,$$

$$c = -_y/_v_d$$

| | |
|---|---|
| A | C j,0 = C inlet |
| B | $(\partial C/\partial y)_{J,k} = 0$, *therefore:* $C_{J-1,k} = C_{J,k}$ |
| C | $J_{y=0} = -D_C \left[\frac{\partial [C]}{\partial y}\right]_{y=0}$ = *heterogeneous rate law* |

Table 1. Boundary conditions for solution of simplified advective diffusion equation.

Boundary conditions are listed in table one for solving equation 6 as a tridiagonal matrix and via the Thomas algorithm. Boundary condition A refers to the upstream boundary (k=0), where it is assumed that reactant concentrations for all j (i.e. Δy). Boundary condition B refers to the plane above the crystal at which vertical transport is no longer important, therefore reactant concentration change with vertical increment change is zero. Boundary C is the crystal surface (j

=0, y=0), change in concentrations at that boundary will be controlled by the rate of reactant reaction at the crystal surface as defined by a heterogeneous rate law.

The Thomas algorithm factors the matrix $T$ into two separate bidiagonal matrices $T_L$ and $T_U$,

$$T = T_L * T_U$$

which are related by the vectors $d$, $f$, and U by the following equations,

| | | |
|---|---|---|
| $d = T\mathrm{U}$ | $f_1 = d_1/\beta_1$ | |
| $T = T_L T_U$ | $f_j = (d_j - (a_j f_{j-1}))/\beta_j$ | for j=2 → J-1 |
| $T_L f = d$ | $\mathrm{U}_{J-1} = f_{J-1}$ | |
| $f = T_U \mathrm{U}$ | $\mathrm{U}_j = f_j - (\gamma_j \mathrm{U}_{j+1})$ | |

and vector elements $\beta_j$ and $\gamma_j$ for $T_U$ and $T_L$ are:

| | |
|---|---|
| $\beta_1 = b_1$ | |
| $\beta_j = b_j - a_j \gamma_{j-1}$ | for j=2 → J-1 |
| $\gamma_j = c_j / \beta_j$ | for j=1 → J-1 |

where J is the maximum division j in the matrix expression. The matrix elements $b_1$, and $d_1$ change for each heterogeneous rate law selected for the calcite surface boundary condition. If the rate law

$$\text{rate (mol cm}^{-2}\text{ s}^{-1}) = k - k' [\mathrm{Ca}^{2+}]_s [\mathrm{CO_3}^{2-}]_s$$

is chosen for the reactant $Ca^{2+}$ at pH 7, the following matrix elements solve the advective diffusion equation by the Thomas algorithm for a $Ca^{2+}$ concentration map, using upstream concentrations $d$ to solve for the immediately downstream vector of concentrations U.

| | |
|---|---|
| $b_1 = a\,(1+(k' \Delta y[\mathrm{CO_3}^{2-}]/D)^{-1} + b$ | for j = 1 |
| $d_1 = \mathrm{C}_{j,k} - (ak\Delta y/D)\,(1+(k' \Delta y[\mathrm{CO_3}^{2-}]/D)^{-1}$ | for j = 1 |

$dj = C_{j,k}$ for j = 2 → J-1

$Uj = C_{j,k+1}$ for j = 1→ J-1

The Thomas algorithm is repeated for each reactant, with the help of Fortran programs available on the world wide web. For carbonate species, only those present in non-negligible concentrations will be considered, for example $H_2CO_3$ would not be considered at pH = 7. Matrix elements $d_1$ and $d_j$ will change for each carbonate species because of homogeneous reactions. Please see Compton and Pritchard, 1990, and Higgins, et al., 2002 for more details on modeling advective diffusion by the Thomas algorithm and determining matrix elements. Once reactant concentrations at the surface are known by agreement of modeled and measured dissolution rates local saturation sate, and nucleation rates of precipitates can be evaluated as well as the local free energy.

A model for calculating non-equilibrium distribution coefficients of solid solutions through consideration of nucleation kinetics from aqueous solutions (Pina, et al., 2002) has been applied to $SrCO_3$ and $BaCO_3$. Nucleation flux (Jx) is very sensitive to changes in composition, so small changes in composition will greatly affect nucleation kinetics of a solid solution – aqueous solution system. Modification of the classic heterogeneous nucleation expression to account for mole fractions between end members yields equation (7), where the subscript x indicates that the pre-exponential factor □, the interfacial free energy □, the molecular volume □ and the super saturation ratio S are functions of the aqueous composition. T is temperature in kelvins, k is the boltzman constant, and B is a shape factor equal to 16/π3 for spherical nuclei or 32 for cubic nuclei.

$$J_x = \square \cdot \exp\left[\frac{\square B \square_x^{3} \square_x^{2}}{k^3 T^3 (\ln S_x)^2}\right] \qquad (7)$$

Consideration of nucleation flux (eq.7) should allow us to predict the location and composition of waste analog precipitates throughout the concentration map provided by modeling.

*Precipitation Characterization by SEM*

Precipitates form on samples with both sufficient divalent metal concentration and exposure times long enough to increase $[CO_3^{2-}]$ so that saturation can be achieved. Figures 4 a and b are SEM electron backscatter images of calcite $\{10\bar{1}4\}$ after exposure to a solution containing 5 mM $Sr^{2+}$, and figures 5 a and b show the same

Figure 4. Electron backscatter images of Sr rich secondry phase on calcite . Sr rich phase seems to decorate steps, predominantly in the [010]. Right: 528 μm wide, 250x, 20kV. Left: 7.33 mm wide, 18x, 20 kV

plane of another calcite crystal after exposure to a 2 mM strontium solution. Bright areas were confirmed to be strontium containing by EDS. Figure 6 shows conditions similar to Figure 4.

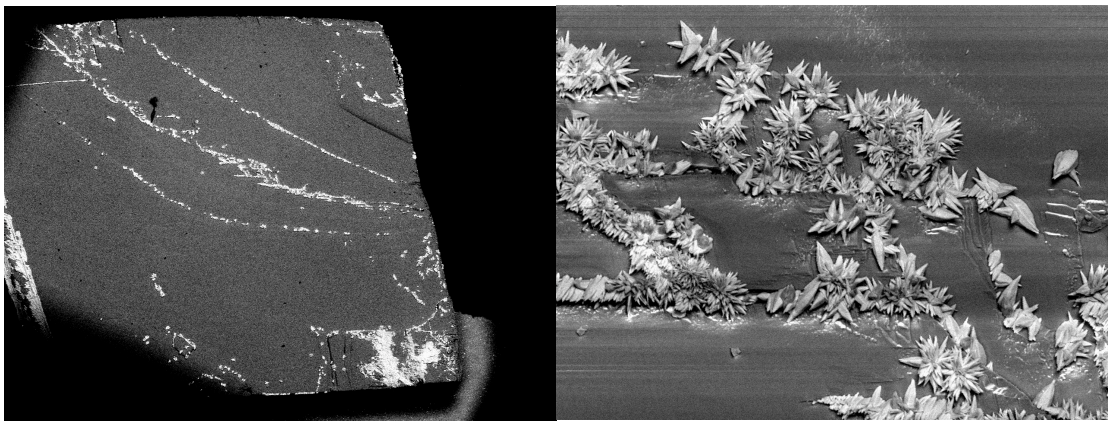

Figure 5. Electron backscatter image of Sr rich crystals at high carbonate flux zones, 2 mM Sr. Right: 489 μm wide, 270x, 20kV. Left:.33 mm wide, 18x, 20 kV

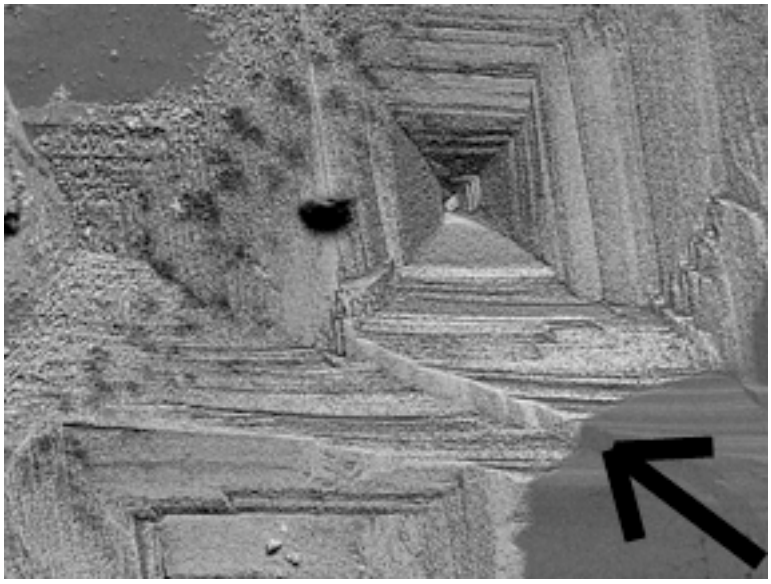

Figure 6: The image above is a backscattered electron image in which light areas indicate the presence of heavier elements. The image is approximately 600 microns along the long axis. X-ray analysis of the light areas reveal the presence of Sr, whereas the darker area shows only Ca. The direction of solution entering the fluid cell through the HAFM inlet jet is indicated.. The inlet solution was 5 mM $SrNO_3$ (i.e., no $CO_3^{2-}$). The image demonstrates the key role of transport, and both spatially and temporally variable conditions, in the study of chemical kinetics in an AFM fluid cell. The area at the arrow that is not covered by the Sr-containing phase is an area of calcite dissolution. As the fluid moves across the surface, its carbonate and calcium concentrations increase because of dissolution. Eventually, at a point indicated here by the light area encountered as the fluid moves away from the inlet jet, the fluid becomes supersaturated with respect to strontianite (probably actually an impure strontianite), and $SrCO_3$ begins to precipitate. We have used the HAFM to image the growth of individual crystals on this sample surface. Further downstream, the fluid approaches saturation with respect to strontianite growth, and further growth ceases. The upstream and downstream edges of the $SrCO_3$ precipitation zone correspond to the spatial points at which the product $[Sr^{2+}][CO_3^{2-}]$ exceeds and lags the strontianite $K_{sp}$, respectively. This in turn places determinable limits on the precipitation kinetics of strontianite in the presence of $Ca^{2+}$ impurities.

Precipitate composition can be evaluated qualitatively based on Lippmann diagrams. (Astilleros, et al., 2002; Lippmann,F., 1980) Figures 7 a and b are Lippmann diagrams for the Sr-Ca-$CO_3$ system. The blue line is a solidus, plot of the log of the summed solubility product ($\sum\prod$) vs mole fraction solid, where:

$$\sum\prod = (K_{cal} * (1-X)*\gamma_{Ca}) + (K_{stron} * X * \gamma_{Sr})$$

$$\sum\prod = (K_{arag} * (1-X)*\gamma_{Ca}) + (K_{stron} * X * \gamma_{Sr})$$

$K_{cal}$, $K_{stron}$, and $K_{arag}$ are the solubiltiy products of calcite, strontianite, and aragonite respectively, while $\gamma_{Ca}$ and $\gamma_{Sr}$ are the rational activity coefficients. The pink and yellow lines are solutus

lines, whose equations are simply the solubility product for the line times the mole fraction of the divalent cation involved in the solubility expression.. For example the rhombohedral calcian solutus (Fig. 7a) would be:

$K_{cal} * (1-X)$ = effective solubility product

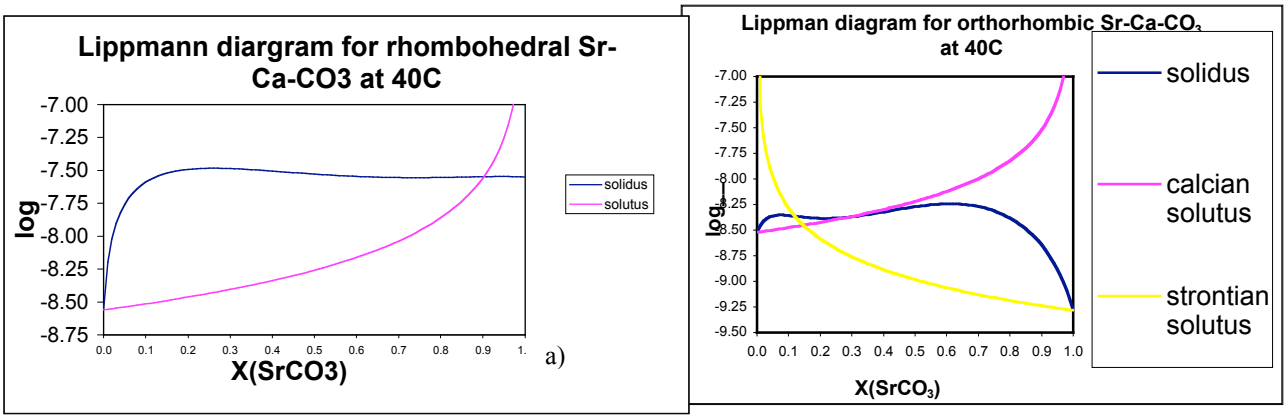


Figure 7 a) Lippman diagram for Sr-Ca-$CO_3$ rhombohedral system at 40 C, b) Lippmann phase diagram for Sr-Ca-$CO_3$ orthorhombic system. Vertical axis is in units of log□□.

The effective solubility product has the same units as □□ and the log is plotted along the same y axis. Solubility products used for 40º C were calculated from 25º C values for Ksp and $\Delta H^0_R$ (Drever,1997) with the Van't Hoff approximation: $K_{cal} = 10^{-8.56}$, $K_{arag} = 10^{8.52}$, $K_{stron} = 10^{-9.28}$.

Considering only the orthorhombic case (Fig. 7b) one can see that a small range of compositional values ($0.85<X<1.0$) for precipitates exists for solutions with high mole fraction Sr. A combination of the rhombohedral case and orthorhombic case reveals that precipitates will be predominately rhombohedral and calcium rich, or orthorhombic and strontium rich.

Similar diagrams can be drawn for the Co-Ca carbonate system (Figure 8 below). Experiments similar to those described above to Sr have been conducted for the Co-Ca carbonate system; some SEM results are presented in Figures 9 and 10 below.

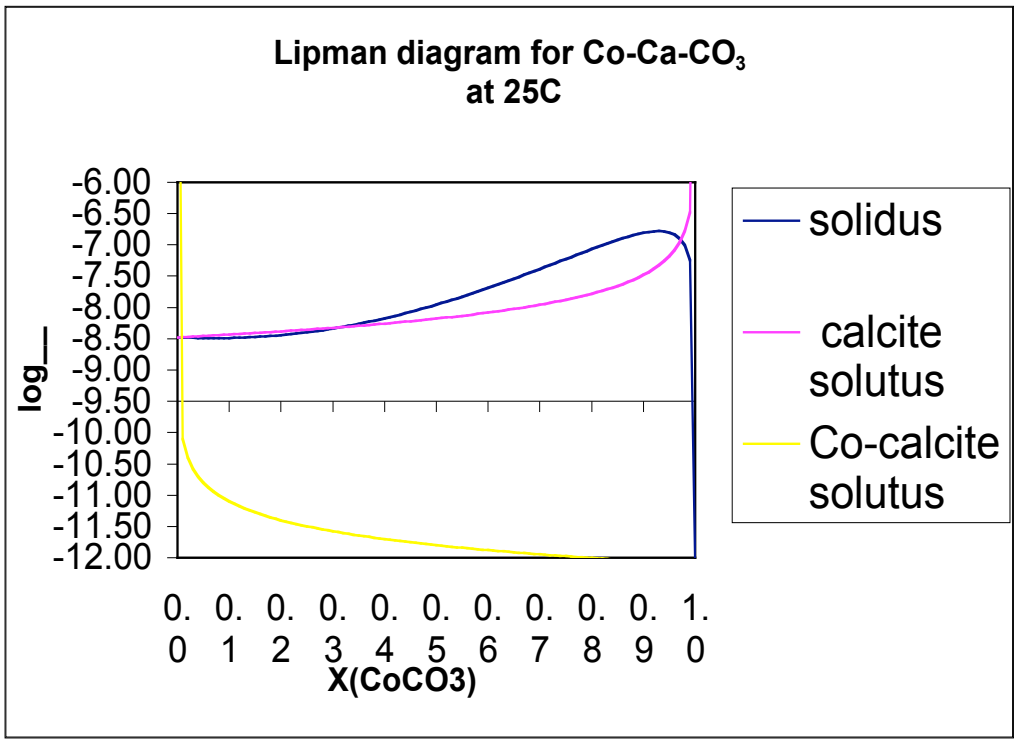


Figure 8. Lippman diagram for the rhombohedral Co-Ca-$CO_3$ system. Vertical axis is log □□

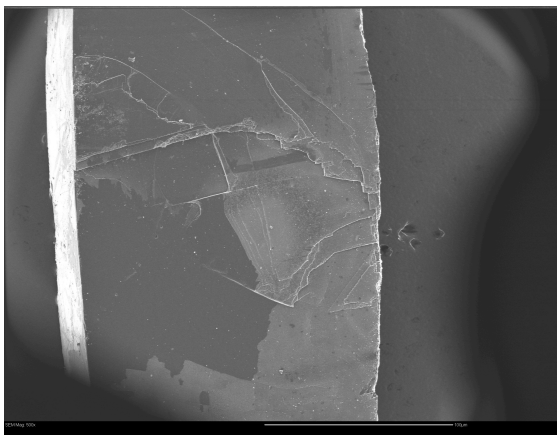

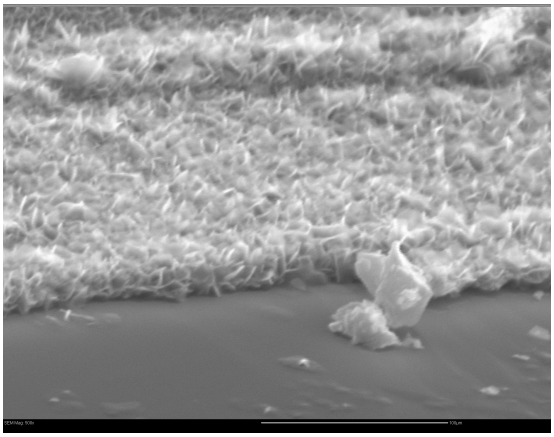

Figure 9. SEM images showing cobalt rich precipitates on the calcite surface after exposure to 0.1 mM $Co^{2+}$ .
Right: Backscatter, 19x, 6.95 mm
Left: Backscatter, 5000x, 26.4 um at a 70º angle

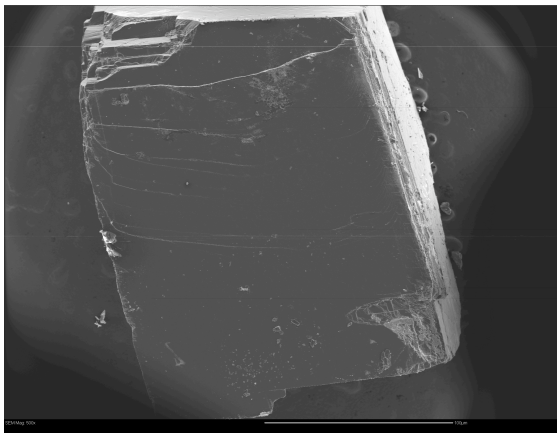

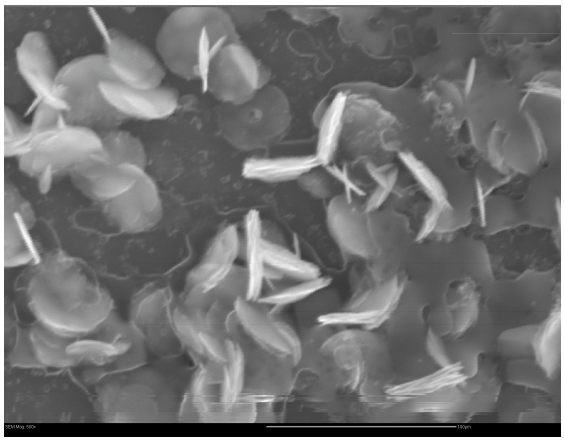

Figure 10. SEM images showing cobalt rich carbonate precipitates on calcite after exposure to 0.05 mM $Co^{2+}$.
Right: secondary electron, 18x, 7.33 mm
Left: Backscatter, 4000x, 33 um

**References:**


Astilleros, J.M.; Pina, C.M.; Fernandez-Diaz, L.;and Putnis, A. (2002) Metastable phenomena on calcite $\{10\bar{1}4\}$ surfaces growing from $Sr^{2+}$ - $Ca^{2+}$ -$CO_3$ aqueous solutions. *Chemical Geology,* Vol. 193, pp. 93-107

Compton, R. G., and Pritchard, K. L., (1990) The Dissolution of Calcite at pH>7: Kinetics and Mechanism. *Phil. Trans. R. Soc. Lond. A*, Vol. 330, pp. 47-70

Drever, J. I. (1997) *The Geochemistry of Natural Waters Surface and Groundwater Environments* Third Ed,. Prentice Hall, Upper Saddle River, NJ

Gratz, A.J., Hillner, P.E., and Hansma, P.K. (1993) Step dynamics and spiral growth on calcite. *Geochem. Cosmochim. Acta* Vol. 57, pp. 491–495.

Higgins, S. R.; Boram, L.H.; Eggleston, C.M., Coles, B.A.; Compton, R.G.; and Knaus, K.G. (2002) Dissolution Kinetics, Step and Surface Morphology of Magnesite (104) Surfaces in Acidic Aqueous Solution at 60º C by Atominc Force Microscopy under Defined Hydrodynamic Conditions. *J Phys. Chem. B* Vol. 106, pp 6696-6705.

Land, T. A. , and DeYoreo, J. J., (1997) An In-Situ AFM Investigation of Canavalin Crystallization Kinetics. *Surf. Sci.* Vol. 384, pp. 136 -155

Lea, A.S., Amonette, J. E., Baer, D. R., Liang, Y., and Colton, N. G.(2001) Microscopic Effects of Carbonate, Manganese, and Strontium Ions on Calcite Dissolution. *Geochim. Cosmochim. Acta* Vol. 65, No. 3, pp. 369 -379

Lide, D. R. (1995) *Handbook of Chemistry and Physics* 76th Ed., CRC Press , Boca Raton, FL

Lippmann, F. (1980)Phase Diagrams depicting aqueous solubility of binary mineral systems, *N. Jb. Miner. Abh.* VoL. 139, PP. 1-25

Lorens, R.B. (1981) Sr, Cd, Mn, and Co distribution coefficiens in calcite as a function of calcite precipitation rate. *Geochim. Cosmochi. Acta* Vol. 45, pp. 553–561.

Nriagu, J. O., (1988) *Chromium in the Natural and Human Environments* 1st Ed. John Wiley and Sons, New York

Pina, C. M., Putnis, A. (2002) The kinetics of nucleation of solid solutions from aqueous solutions: A new model for calculating non-equilibrium distribution coefficients. *Geochim. Cosmochim. Acta*, Vol. 66, No.2, pp. 185-192.

Pingitore, N.E. Jr., Lytle, F.W., Davies, B.M., Eastman, M.P., Eller, P.G. and Larson, E.M. (1992) Mode of incorporation of $Sr^{2+}$ in calcite: Determination by X-ray absorption spectroscopy. *Geochim. Cosmochim. Acta* Vol 56, pp. 1531–1538.

Reeder, R.J. (1983) *Reviews in Mineralogy Vol. 11 Carbonates: Mineralogy and Chemistry* MSA, pp. 1–47

Teng, H.H., Dove, P.M., and DeYoreo, J.J. (2000) Kinetics of calcite growth: Surface processes and relationships to the macroscopic rate laws. *Geochim, Cosmochim. Acta* Vol. 64, pp. 2255–2266.

US DOE (2000) Vadose Zone Fact Sheet, Hanford Site. *www.em.doe.gov/ftplink/vadose/Hanford.pdf*